On the Wall Slip of Polymer Blends

A. MACIEL,[1] V. SALAS,[1] J. F. A. SOLTERO,[2] J. GUZMÁN, O. MANERO[1]

[1]Instituto de Investigaciones en Materiales, Universidad Nacional Autónoma de México (UNAM), A.P. 70-360, México, D.F. 04510, México

[2]Departamento de Ingeniería Química, Universidad de Guadalajara, Blvd. M. García Barragán 1451, Guadalajara, Jal. 44430, México

Received 23 April 2001; revised 13 November 2001; accepted 15 November 2001

ABSTRACT: The slip flow of the polypropylene (PP)/poly[ethylene-*co*-(vinyl acetate)] (EVA) system was studied in a capillary rheometer for shear rates of 40–1000 s^{-1} at four temperatures. Three dies made of aluminum with a length/diameter (L/D) ratio of 15 and diameters of 1.59, 1.19, and 0.79 mm provided the flow data. Calculations of the slip velocity by the Mooney method showed power-law behavior with the stress. Blends were prepared at various proportions of PP and EVA for observation of the variation of the slip velocity for different compositions and temperatures. Direct microscopic observations of the slip layer on extruded samples showed domains of the dispersed phase unevenly distributed between the slip layer and the core and provided estimates of the thickness of the layer adjacent to the capillary wall. Results showed that the viscosity in the slip layer was 10–100 times lower than that in the bulk for the same value of the shear stress. In terms of the extrapolation length, the development of the slip layer was the result of different disentanglement dynamics of the molecules in the slip layer in comparison with those in the bulk. © 2002 John Wiley & Sons, Inc. J Polym Sci Part B: Polym Phys 40: 303–316, 2002; DOI 10.1002/polb.10093

Keywords: wall slip; capillary rheometry; polymer blends; Mooney analysis; extrudate morphology; interfacial slip

INTRODUCTION

The apparent slip in polymer melts has been much studied in recent years, and special attention has been given to the extrusion defects observed in the capillary flow of highly viscous polymer systems. Recent review articles[1,2] highlight the importance of fundamental research in understanding the relation of slip flow to extrudate distortion. The general view is that the fluid layer adjacent to the wall in capillary flow develops characteristics different than those of the bulk flow. An abnormal decrease in the viscosity brought about by high-velocity gradients in this layer is observed, and this effect is more pronounced in smaller capillaries (i.e., those with smaller diameters). The resulting flow curves show a consistent increase in the velocity gradient for a given stress as the capillary diameter diminishes.

In the absence of end effects, the viscosity calculated from flow curves of capillaries with relatively large diameters coincides with the true flow curve, implying that the wall effects in this case are negligible. However, as the diameter diminishes, the wall layer becomes increasingly important, and corrections to the data are necessary. Mooney[3] suggested a method of correcting flow curves (shear stress vs shear rate) with at least

Correspondence to: O. Manero (E-mail: manero@servidor.unam.mx)

Journal of Polymer Science: Part B: Polymer Physics, Vol. 40, 303–316 (2002)

three capillaries of different diameters. A characteristic velocity, that is, the slip velocity (V_s), is associated with the increment of the velocity gradient for a given stress as the diameter diminishes. If the velocity-gradient increment is linear with the inverse radius, extrapolation will give the true wall shear rate. V_s can then be estimated from the slope of the curve for each shear stress. A power-law relationship has been found for the V_s variation with the shear stress in most cases.

The existence of the apparent slip or low-viscosity layer adjacent to the wall has been given several explanations. The migration of low molecular weight species to regions of high shear rates (or the depletion of high molecular weight components in the region close to the wall) has been proposed to account for such low-viscosity regions. Studies were performed to determine the molecular weight of concentric layers of extrudate. Only differences up to 4% were measured in polydisperse polystyrene[4] between the central and wall regions. A low-viscosity layer at the wall was found in poly(vinyl chloride) (PVC),[5] consisting mostly of low molecular weight additives. In this system, low molecular weight PVC did not exhibit slip, in contrast to high molecular weight PVC.[6] Slip was modified or prevented with changes in the wall roughness or material.[7–12]

Wall slip has been considered a possible explanation for the multiple values of the shear-rate/shear-stress flow curve,[13] often called *inherent constitutive instabilities*.[14] According to this hypothesis, a single shear stress may correspond to at least two values of shear rate, the lower value corresponding to the bulk flow and the larger one corresponding to the wall region. The region adjacent to the wall will present a lower viscosity if the fluid is shear-thinning. Sometimes the span of the multiple-value region is large, and the increases of the wall shear rate are in the form of jumps or spurts as the driving pressure gradient is increased beyond a critical value.

The presence of regions of more aligned (or more disentangled) molecules within low-viscosity regions and a more viscous bulk fluid with less aligned molecules for a given shear stress in capillary flow reflects the existence of a flow curve with a stress plateau or flow curves containing maxima and minima. This leads to different rates of entanglement and disentanglement of chains in the bulk in comparison with those at the wall. Experimental verification of such issues is the subject of this work. If direct observations of the width of the slip region are made and V_s is available (e.g., by the Mooney method), the shear rate at the wall can be estimated for a given stress. Alternatively, one can calculate the extrapolation length as a function of shear stress, as defined elsewhere.[15] If a slip layer develops, differences between the values of the shear rate at the wall and the shear rate in the core for a given stress lead to different viscosities in the fluid in contact with the wall and in the fluid in the capillary center. This experimental fact reveals the multiple values of the flow curve. A polymer blend, which may segregate or demix under capillary flow, is required for this. To this end, polypropylene (PP)/poly[ethylene-*co*-(vinyl acetate)] (EVA) blends, immiscible systems with components of different glass-transition temperatures, were used in this analysis. The slip-layer width (δ_s) was determined through observations by scanning electron microscopy on extruded samples for various temperatures and compositions.

EXPERIMENTAL

Materials

Isotactic PP from Himont with a molecular weight of 228,000 [number-average molecular weight (M_n) = 28,900] was used in the experimental work. It had a melting temperature of 173 °C and a melt flow index of 3. EVA from Elf Atochem with a molecular weight of 125,700 (M_n = 48,000) had a melting temperature of 76 °C and a melt flow index of 5.

Equipment

Blends were prepared in a Haake Rheocord-254 single-screw extruder (L/D = 25:1). The polymers were extruded in the form of a plane sheet. Then, they were pelletized and extruded once more to produce pellets for the capillary viscometer. Extrusion temperatures were 210, 220, and 225 °C.

The samples were placed in the barrel of an Instron 3210 capillary viscometer provided with three capillaries (L/D = 15, entry angle = 180°). Capillary diameters were 1.59, 1.19, and 0.79 mm. Experiments were performed with a height of the sample in the chamber of 10 cm, and special care was taken to avoid the presence of bubbles in the extruded samples.

For the evaluation of end effects in the capillary flow of the blends, rotational viscometry measurements in a cone-and-plate apparatus (Rheo-

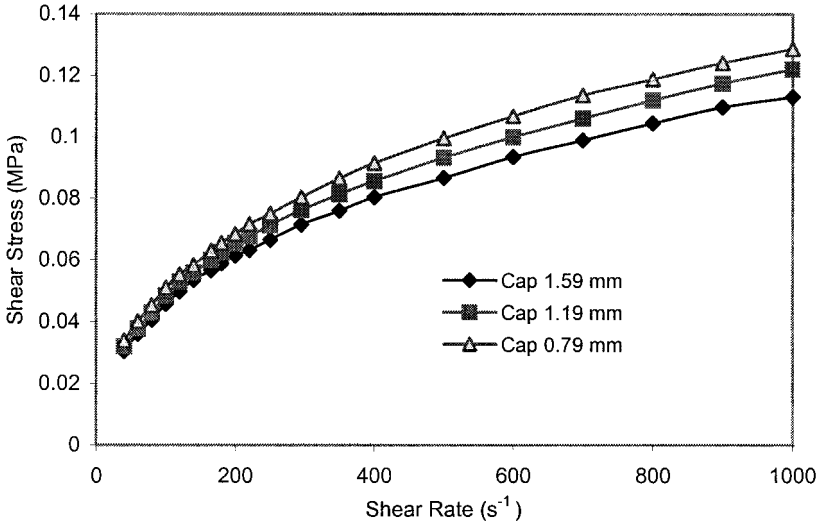

Figure 1. Apparent stress versus the apparent shear rate for the 90/10 PP/EVA blend at 225 °C with three different diameters and the same L/D.

metrics RDS II; radius = 2.5 cm, angle = 0.1 rad) were compared to those made in the capillaries. The method of evaluating these effects is described later.

Morphological features of the blends extruded from the capillary were analyzed with a scanning electron microscope (Laica Stereoscan 440). The exterior and transverse surfaces of samples extruded from the largest capillary were observed. For the transverse-surface studies, the extruded filaments were fractured after immersion in nitrogen. Thereafter, the samples were immersed in toluene for 48 h for extraction of the EVA phase and then were gold-coated for the microscopy studies. Observations of the core of the filament, the wall region, and the intermediate region provided information on the morphological features of the dispersed phase.

Microscopy studies were complemented by optical microscopy observations with crossed polarizers for distinguishing differences in the birefringence patterns between the observed regions. Samples were prepared with cryogenic ultramicrotomy (Research & Manufacturing Co., MTX).

Flow curves were obtained in the capillary viscometer for pure PP and 95/5, 90/10, 85/15, and 50/50 (w/w) PP/EVA blends at 190, 200, and 225 °C in a shear-rate range of 40–1000 s^{-1}.

RESULTS

From data of the pressure versus the flow rate, the shear-stress/shear-rate flow curve was obtained, with the following relationships for pipe flow:

$$\text{Shear stress:} \qquad \tau = \frac{\Delta p - \Delta p_{\text{ent}}}{2\left(\frac{\text{L}}{\text{R}}\right)} \tag{1}$$

$$\text{Apparent shear rate:} \qquad \dot{\gamma}_{\text{app}} = \frac{4Q}{\pi R^3} \tag{2}$$

where the pressure drop (Δp) is calculated from the steady-state value of the measured piston force and Δp_{ent} is the excess pressure due to entrance effects. Q and R are the flow rate and capillary radius, respectively. Figure 1 shows the apparent shear stress (calculated from the total pressure drop) versus the apparent shear rate for several diameters (L/D = 15) for a 90/10 PP/EVA blend at 225 °C. Diameter-dependent shear rates $\dot{\gamma}(D)$ are shown for each stress. Higher shear rates correspond to smaller diameters, illustrating what is usually termed *apparent slip*. A quantitative evaluation of these effects may be accomplished with the well-known Mooney method.[3] With the curve with the largest diameter taken as a reference, if slip effects in this capillary are negligible, the abnormal larger shear rates in the smaller capillaries can be quantified. For a given stress, in terms of apparent shear rates, the difference between the reference shear rate ($\dot{\gamma}_{\text{ref}}$) and $\dot{\gamma}(D)$ is characterized by V_s and the characteristic length scale, which is the diameter of the

capillary with slip effects (D). In mathematical terms, this is written as

$$\dot{\gamma}(D) - \dot{\gamma}_{ref} = 8V_s/D \quad (3)$$

From a set of capillaries with different diameters but the same L/D, a plot of $\dot{\gamma}(D)$ as a function of $1/D$ will be a straight line with slope $8V_s$ and intercept $\dot{\gamma}_{ref}$. This procedure is based on the assumption that the capillary with $\dot{\gamma}_{ref}$ has a sufficiently large diameter that the ratio of the characteristic length of the slip layer (its width) to the capillary diameter is negligible, and so slip effects are negligible. The problem here is that we do not know a priori, for any complex flow, the correct diameter. If this capillary is not chosen correctly, eq 3 will show a departure from the straight line, which is additionally complicated by the presence of entrance effects. In fact, eq 3 holds in the fully developed flow region of the capillary; therefore, a key assumption of the Mooney technique is that V_s is a unique function of the true wall shear stress. Surprisingly, eq 3 has often been used without proper consideration of the end effects. Because the characteristic length of the entrance region is not known a priori, it is necessary to evaluate end effects, in this case entrance effects, to ensure that eq 3 is applicable to the flow data. This is usually accomplished with the Bagley correction, in which the variation of Δp with L/D for several capillaries gives an additional equivalent L/D contribution (at a constant shear rate) to the stress of eq 1 due to entrance effects. In this work, the implementation of this procedure would be cumbersome because of the large number of measurements at several temperatures and compositions needed. Instead, the evaluation of entrance effects was performed with a comparison of the capillary flow data with the complex viscosity curve. Under the assumption that the Cox–Merz rule was applicable (i.e., the numerical equivalence of the complex viscosity and the steady shear viscosity), capillary flow data were compared with the oscillatory cone-and-plate data. In this comparison, regions of overlap were sought for the reduction of experimental uncertainties. In Figure 2(a,b), this comparison is performed for pure PP at 190 °C. In Figure 2(a), entrance effects account for deviations seen for a shear-rate range of 100–1000 s^{-1}. Because slip effects and end effects are coupled in a complex manner, we have to follow an iterative procedure by which Δp_{ent} (eq 1) is assumed as a first approximation. Then, the Mooney correction is performed with the assumed true stress, and the true wall shear rate is calculated after the Rabinowitsch correction is performed for non-Newtonian effects. If the assumed excess pressure is correctly guessed, capillary data will superpose and continue the trend of the complex viscosity, as shown in Figure 2(b). In following this procedure, we can also determine if the capillary with negligible slip effects has a diameter large enough to be the capillary for $\dot{\gamma}_{ref}$.

Corrections for slip and end effects were performed on the blends for all concentrations and temperatures considered in this work. In all cases, the stress and shear rates follow a power-law relationship. The Rabinowitsch correction for these fluids was used:

$$\dot{\gamma}_w = f_n \, \dot{\gamma}_{ref} \quad (4)$$

where

$$f_n = (3n + 1)/4n \quad (5)$$

$\dot{\gamma}_w$ is the true shear rate at the wall, n is the power-law index, and the apparent shear rate $\dot{\gamma}_{ref}$ is given in eq 3.

In Figure 3, Mooney plots for pure PP at 190 °C are shown. Within experimental error, straight lines are only obtained at low stresses. These curves (in the low-stress region) provide values of V_s and corrected shear rates for the blends at several temperatures and for various compositions. The dependence of V_s on temperature and composition was given attention by Valdez et al.[16] They found maxima in V_s as a function of composition in biopolymer systems. Magnitudes of the slip velocities are similar to those obtained by Jiang et al.[17]

In the range of temperatures studied (190–225 °C) and in the dilute concentration range (0–15 wt % EVA), the power-law index was quite constant and equal to 0.36 ± 0.02. This suggests that it is possible to perform a time–temperature superposition analysis on the corrected flow curves for several temperatures and compositions in a specific range. The shift factors are defined as follows:

$$\text{Temperature shift factor:} \qquad a_T = \frac{\dot{\gamma}(T_0)}{\dot{\gamma}(T)} \quad (6)$$

$$\text{Concentration shift factor:} \qquad a_C = \frac{\dot{\gamma}(C_0)}{\dot{\gamma}(C)} \quad (7)$$

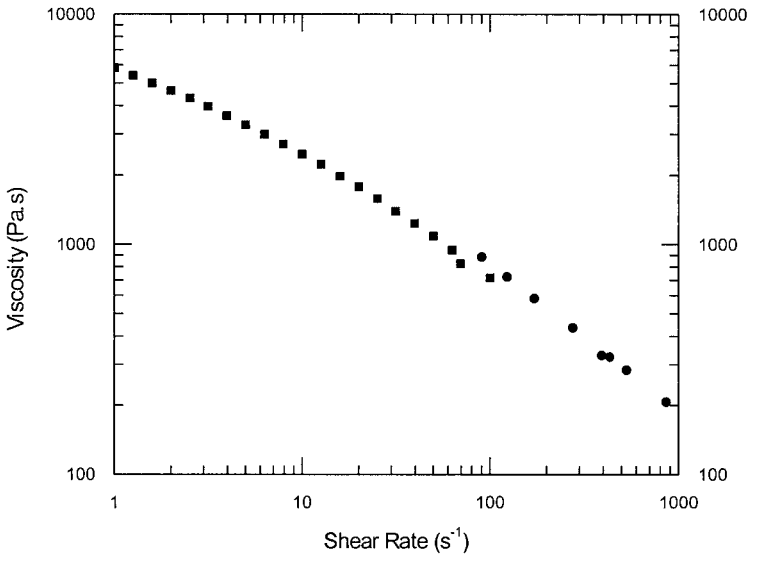

(a)

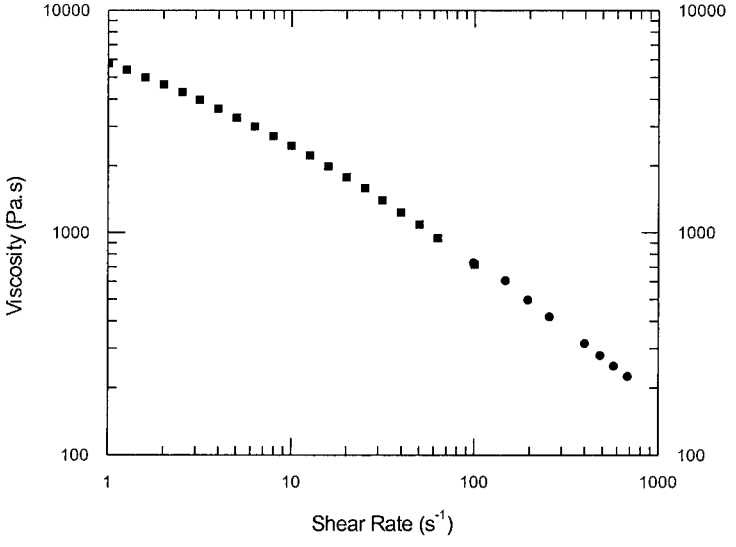

Figure 2. Complex viscosity versus the frequency (■) plotted with capillary data (●) at 190 °C: (a) capillary data without correction for entrance effects and (b) capillary data with correction for entrance effects.

Master curves were constructed, with the reference temperature and concentration T_0 = 190 °C and C_0 = 100 wt % PP, respectively. Furthermore, an overall master curve embodying individual master curves was constructed for the viscosity/shear-rate and slip-velocity/shear-stress relationships, respectively. The results of this analysis are presented in Figures 4–6.

Figure 4 shows the viscosity/shear-rate curve, in which complex viscosity data for pure PP at 190 °C are plotted along with the global master curve resulting from time–temperature–concentration superposition (reduced to 100 wt % PP and 190 °C). Although the scatter indicates a lack of superposition and experimental errors in the measurements and the reduction procedure, the

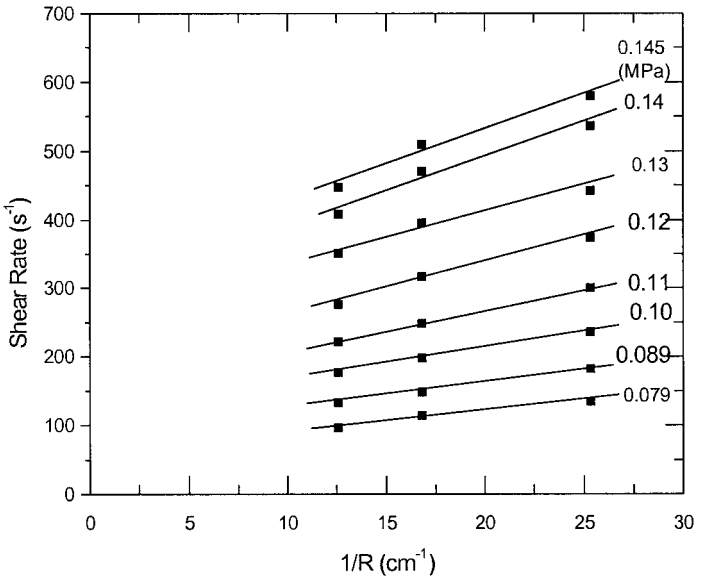

Figure 3. Mooney plots for pure PP at 190 °C for several shear stresses.

capillary data overlap and continue the trend of the complex viscosity. We expected such an error because corrections to the stress and shear rate were performed for each concentration and temperature, followed by a two-stage superposition. Furthermore, in general, immiscible polymer blends do not follow time–temperature superposition because of the different relaxation modes of each polymer. We may expect a degree of superposition if the concentration of one phase is small within a narrow temperature span. The temperature shift factor (a_T) and concentration shift factor (a_C) used in the superposition are illustrated in Figure 5(a,b). a_T follows a near-Arrhenius be-

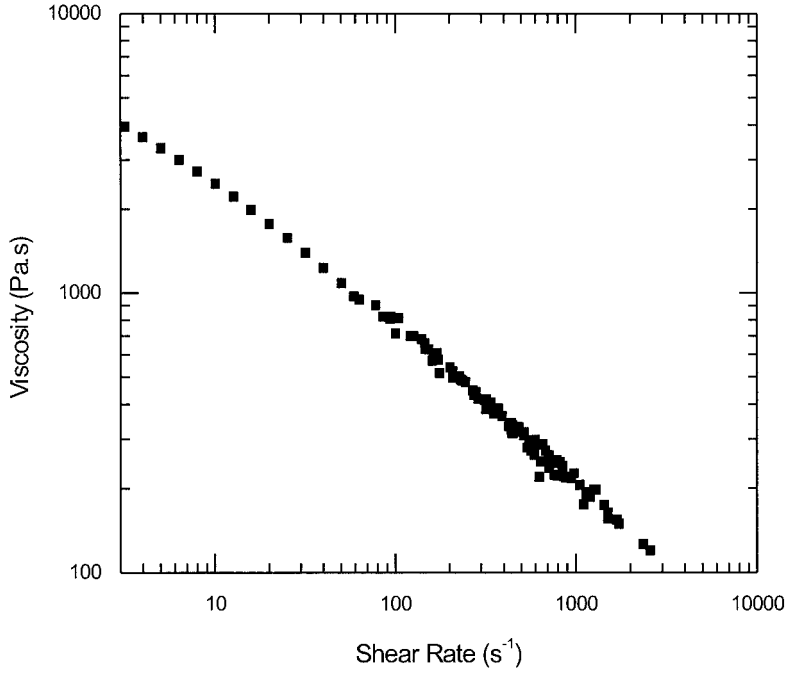

Figure 4. Complex viscosity versus the frequency for pure PP at 190 °C plotted with the master curve from capillary data reduced to 100 wt % PP and 190 °C.

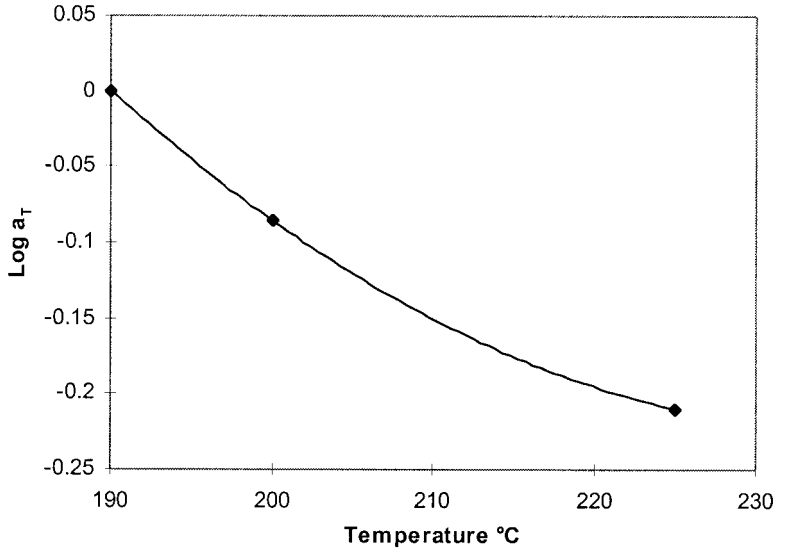

(a)

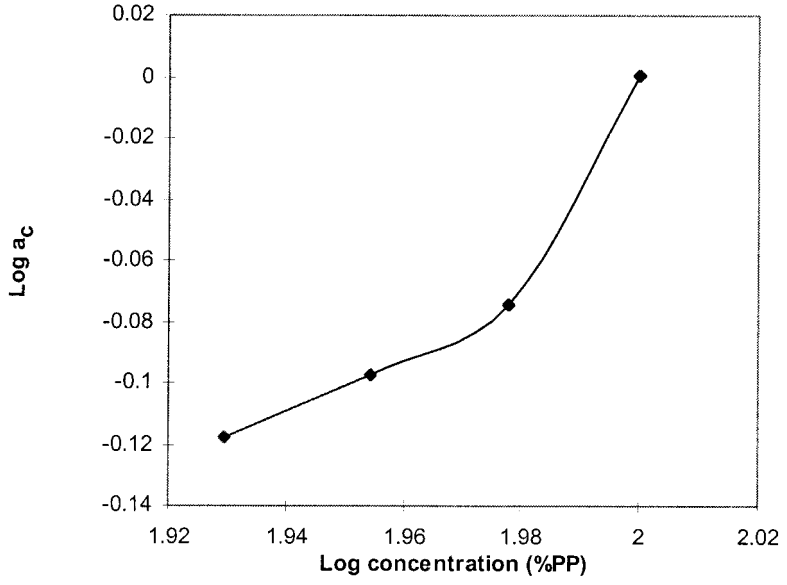

(b)

Figure 5. (a) a_T and (b) a_C for the viscosity/shear-rate master curves.

havior close to a Williams–Landel–Ferry function, and a_C approaches a slope of 0.75 as the EVA concentration decreases.

In Figure 6, V_s is plotted with the shear stress. The slope of this curve is 2.5. Similar values have been reported in the literature for polymer melts.[2] The shift factors implied in the construction of Figure 6 indicate a near-exponential variation of a_T and a stronger variation with concentration of a_C than that in the bulk. Thus, the concentration dependence in the slip layer is more pronounced than that in the bulk.

To analyze the morphology and length scales of the slip layer as functions of temperature and composition of the EVA/PP blends, we took a series of micrographs of several samples in which EVA was the dispersed phase. The micrographs shown in Figures 7(a–c) illustrate the morphology in the wall region, intermediate region, and capillary center, respectively. These micrographs were taken of a blend with an 85/15 PP/EVA composition at 190 °C with a shear rate of 40 s^{-1}. The wall region shows a skin with no EVA domains and features quite different than those

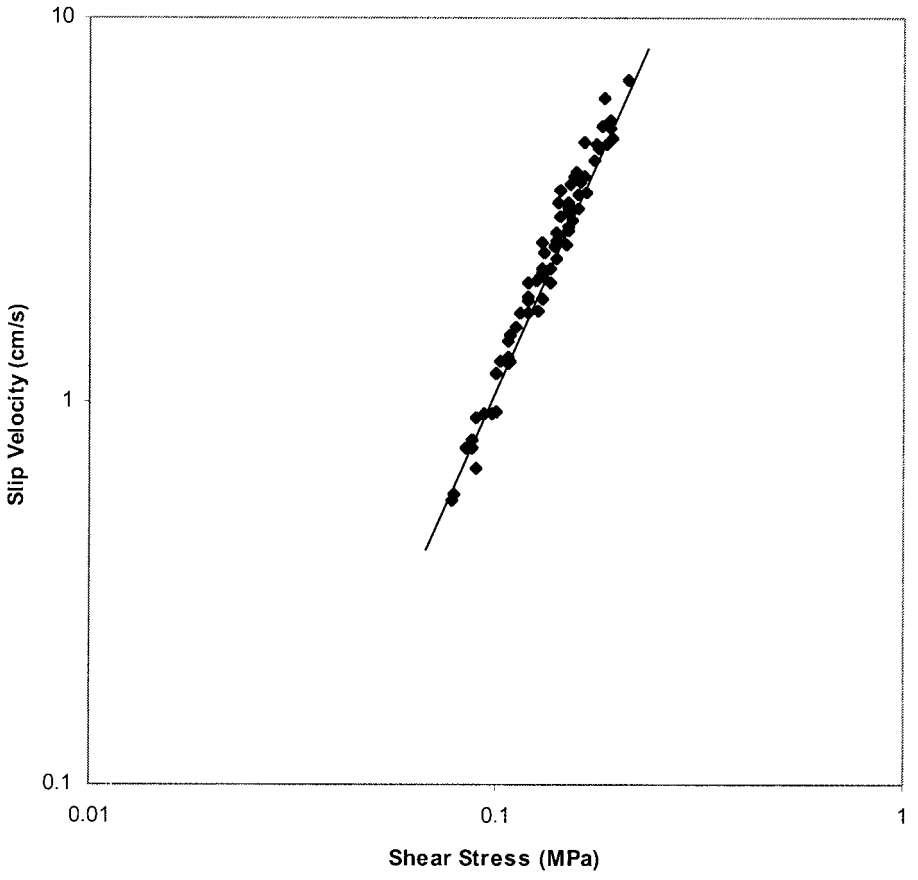

Figure 6. Slip velocity plotted with the shear-stress master curve reduced to 100 wt % PP and 190 °C.

found in the inner regions. The width of this region is only 1 μm. Adjacent to the wall region there is a layer in which again no EVA domains are observed. The intermediate region shows EVA domains of approximately 0.5 μm. The core region has EVA domains of 1 μm. As the shear rate is increased, the size of the dispersed-phase domains in the core region decreases to 0.75 μm. Variation of the domain size with shear stress has been observed by others in similar systems.[18]

An interesting observation is the presence of domains deformed along the angular direction of the extrudate. It seems that the extrudate rotates as it is pushed out of the capillary. It is not possible to confirm whether this occurs inside the capillary or is due to polymer relaxation outside the capillary. Alternatively, one may think of an effect of the stresses developed as the free surface evolves right at the exit of the die. Some authors attribute the spiral-like extrudate distortion of PP and other polymers to a secondary (vortex) flow in the barrel due to a sharp die entry.

It is also noteworthy that the filament that leaves the capillary at the initiation of flow (when the force has not achieved steady-state conditions) has a morphology different than that observed under steady-state conditions. In this case, the wall-layer width is 10 μm with dispersed EVA microdomains. It is apparent that the morphology develops on the same timescale as the approach of the force to the steady state. Apparently, the uniform distribution of EVA domains in the filament existing at the initiation of flow changes with time and leads to a depleted layer close to the wall. EVA domains either are broken into submicrometer-size particles (not observable) or are highly deformed into very thin filaments. The migration of particles to the core region may also cause the resulting morphology. In any of these situations, a depleted PP layer adjacent to the wall is the characteristic pattern at this concentration.

To investigate this effect further, we considered a blend with a larger EVA content in which

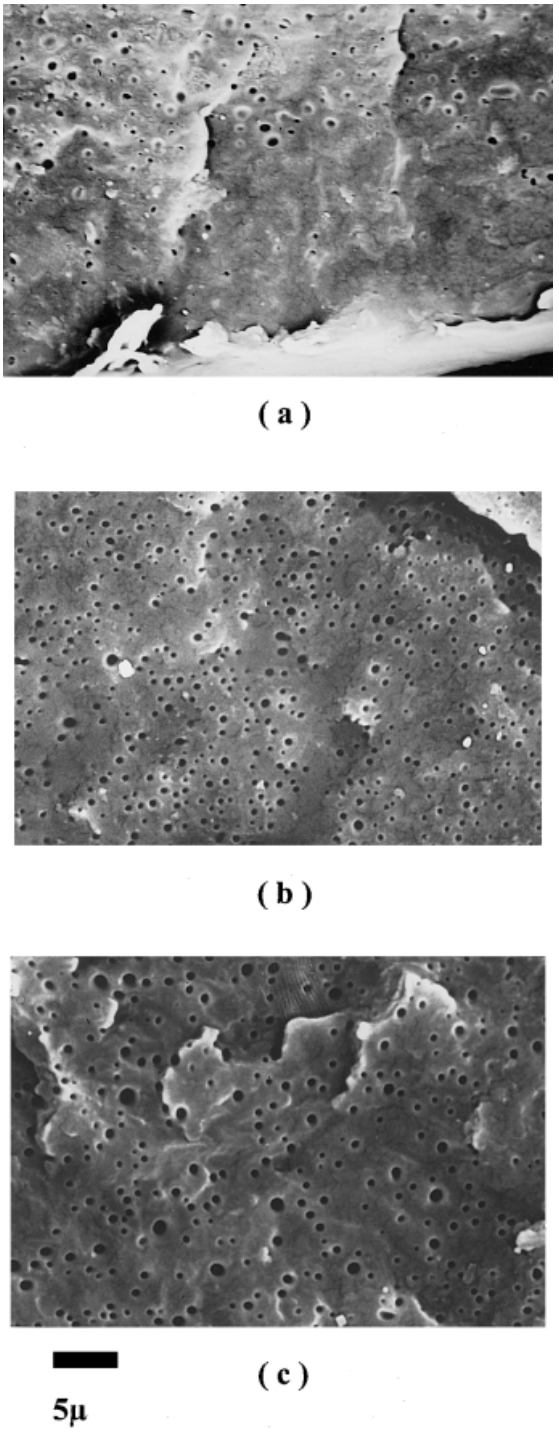

Figure 7. Morphology of the PP/EVA blend taken at 190 °C and 40 s^{-1}: (a) at the wall region, (b) intermediate, and (c) center of the capillary.

the EVA phase was the continuous phase. In Figure 8, a blend with 85–15% EVA/PP has a slip layer 3 μm in width depleted of the dispersed phase with particle sizes increasing for smaller radial distances. As in the PP-continuous phase blends, the morphology in samples taken at the initiation of flow exhibits domains present in the slip layer.

An interesting case is the morphology shown by the 50–50 PP/EVA blend. At a shear rate of 900 s^{-1}, the slip layer has domains of EVA and PP with a width of 26 μm. This blend develops the largest V_s value at 190 °C.

From the micrographs shown in Figures 9(a–c), we seek a relationship between the shear rate and δ_s. The blend composition is 90/10 PP/EVA at 225 °C. As the shear rate increases from 40 to 1000 s^{-1}, δ_s decreases from 1.5 μm (40 s^{-1}) to 0.3 μm (1000 s^{-1}). An intermediate size of 1 μm is measured at 400 s^{-1}. Such a relationship does not hold for varying blend composition. From 100 to 85% PP contents, at 225 °C no correlation exists between the composition and δ_s. The magnitude of the slip layer changed from 1 μm for 100 and 95% PP to 300 nm for 90% PP and to 3 μm for 85% PP. The 90% PP blend had the smallest width but the highest V_s. In Table I, the width of the wall layer is shown for blends with various temperatures and compositions.

Polarized optical microscopy confirmed the results of the analysis made by scanning electron microscopy. Similar morphology patterns of multiphase polymer blends have been observed by several other authors.[19–21]

The observed variation of the wall-layer width with the shear rate (or applied stress) suggests that the representative shear rate at the wall increases with the reduction in layer width. This can be expressed as follows:

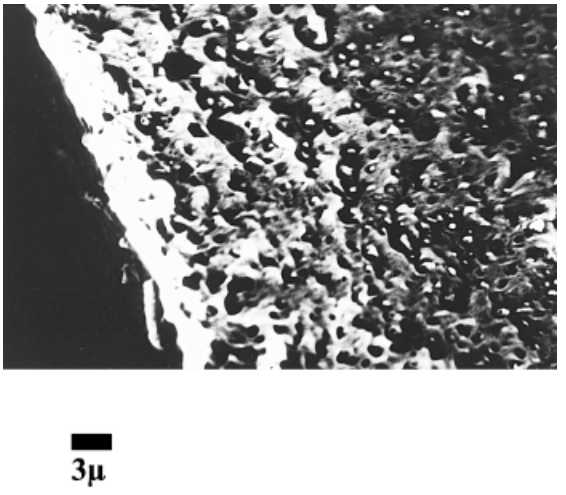

Figure 8. Slip-layer morphology for 85/15 EVA/PP at 180 °C.

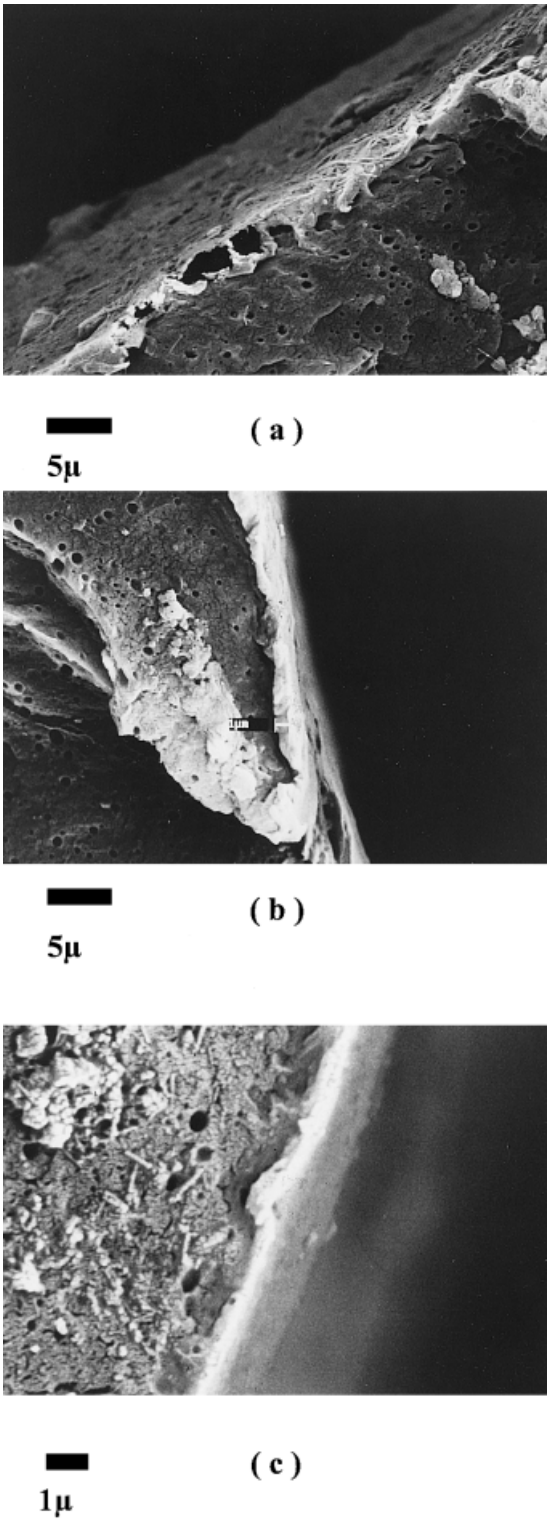

Figure 9. Width of the slip layer for the 90/10 PP/EVA blend at various shear rates: (a) 40, (b) 400, and (c) 1000 s^{-1}.

$$\tau = \frac{\Delta p}{2\left(\frac{L}{R}\right)} = \eta_s \left(\frac{V_s}{\delta_s}\right) \tag{8}$$

where the representative shear rate at the wall is given by the ratio of V_s to δ_s. Equation 8 further indicates that the viscosity in the wall layer (η_s) is given by the ratio of the wall stress and the representative shear rate. This expression was suggested by Jiang et al.[17] and accounts for a drastic reduction in the viscosity of the slip layer in comparison with that in the core region. This is clearly observed in Figure 10, in which the viscosity of the fluid adjacent to the wall decreases very rapidly with the representative shear rate V_s/δ_s. In fact, the slope of this curve is close to -1, a signature of pronounced shear thinning. Although there is a quite large scatter in the wall shear rate due to a lack of precision in the measurements of δ_s, the magnitude of the wall shear rate is certainly much larger than the bulk shear

Table I. Slip-Layer Width (δ) for Various Shear Rates and Temperatures for Pure PP and PP/EVA Blends

τ (MPa)	$\dot{\gamma}$ (s^{-1})	V_s/δ (s^{-1})	δ_s (μ)
190°C			
85%PP			
0.0512	40	976	1
0.1275	400	19,500	1
0.1754	1,000	44,600	1.3
90%PP			
0.1741	1,000	15,050	2
100%PP			
0.1947	1,000	35,185	2
50%PP			
0.1825	900	4,079	26
225°C			
85%PP			
0.1265	1,000	17,467	3
90%PP			
0.0316	40	840	1.5
0.0913	400	31,600	1
0.1287	1,000	227,000	0.3
95%PP			
0.1342	1,000	54,800	1
100%PP			
0.1461	1,000	89,800	1
180°C			
15%PP			
0.1465	400	7,400	3

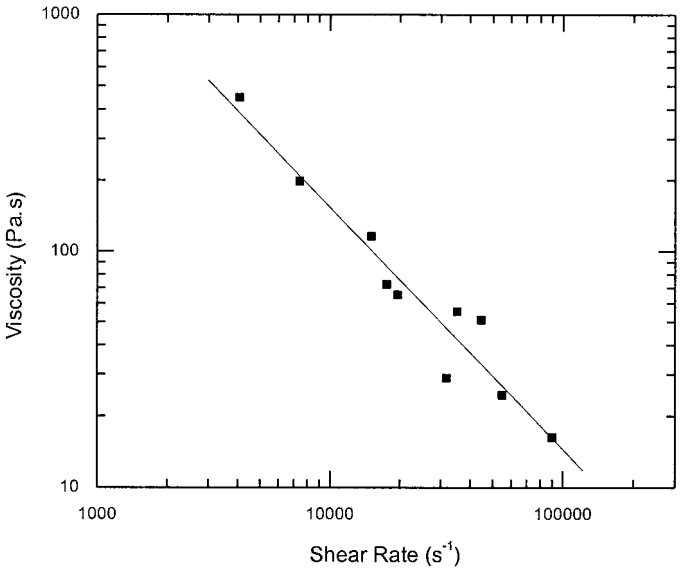

Figure 10. Variation of the viscosity of the slip layer with the interfacial shear rate (V_s/δ_s).

rate. To illustrate the span of shear rates existing in the wall region compared with those in the bulk, in Figure 11 we have plotted the true wall shear stress versus the true wall shear rate. In the same figure, we have plotted the shear rates representative of the slip layer. The latter span the high-shear-rate region with an average plateau stress, whereas the bulk data at low shear rates follow a uniform power-law relationship. When they are plotted together, discontinuities at a critical stress (or critical shear rate) and multiple values of the shear stress/shear-rate relationship are observed. Furthermore, the viscosity in the wall region may be 2 decades smaller than the viscosity in the bulk. In Figure 11, we have plotted the true wall shear stress versus the true wall shear rate corrected for entrance pressure drop, non-Newtonian flow, and slip. The result is the true flow curve for the bulk polymer, which is continuous and monotonically increasing. In the

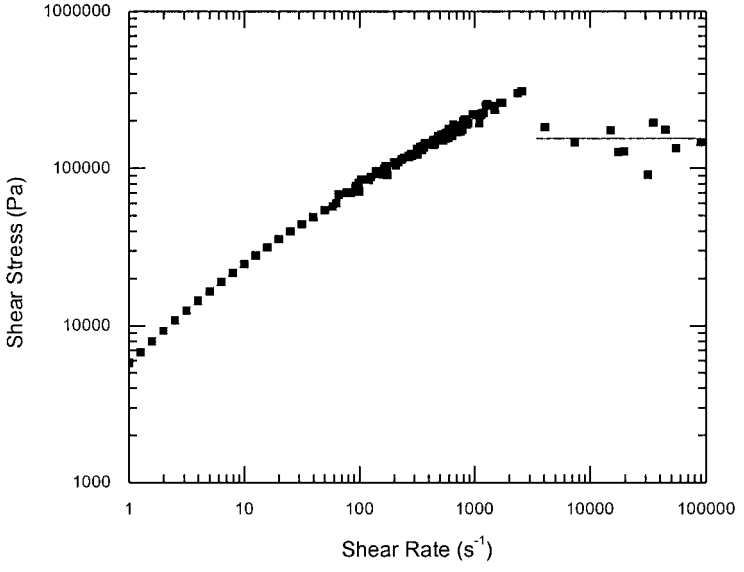

Figure 11. True shear stress as a function of the true shear rate in the bulk plotted with slip-layer data (shear rate = V_s/δ_s). Complex viscosity data are included.

same figure, we have plotted the interfacial shear rate at the wall (V_s/δ_s) calculated for a given stress. The hypothesized multiple values of the curve arise from the two values of the shear rate for a given stress: the true shear rate in the bulk and the interfacial shear rate given in eq 8. Data in Figure 11 correspond to values taken at several concentrations and temperatures, and so the extent of the plateau region will depend on a particular temperature and concentration.

These results suggest that the velocity profile in the capillary in the fully developed region consists of a flattened core occupying most of the transverse area and a very thin layer adjacent to the wall in which the velocity decreases abruptly to zero. The profile looks like a quasisolid displacement of fluid that actually slips at the capillary walls. As a function of time, the profile will evolve from a parabolic profile at the onset of flow into a flattened profile in the steady-state equilibrium flow. Therefore, the distribution of the dispersed phase domains is uniform in the initial transient flow but segregates during the timescale of the formation of the slip layer as soon as a critical stress is attained. The critical stress may be as low as 50 kPa (see Table I), at which point we observe the development of the slip layer.

Alternative explanations for the data presented in this article have been proposed.[1,11,22] We discuss here the results in terms of the Navier–de Gennes[15] concept of interfacial slip. In this, a slip hydrodynamic boundary condition is introduced in which V_s at a solid/liquid interface is determined by the shear stress at the wall:

$$\tau = \beta V_s \tag{9}$$

where β is the interfacial friction coefficient that characterizes viscous interactions at the boundary. The Navier–de Gennes extrapolation length (b) arises as a length scale in the analysis of flow behavior in the presence of slip:

$$b = V_s/\dot{\gamma} \tag{10}$$

where the shear rate in the bulk is implied in eq 10. It follows that

$$b = \eta/\beta \tag{11}$$

where η is the bulk viscosity. In the systems treated in this work, the friction coefficient for various temperatures and concentrations may be extracted from Figure 6. The stress follows a power law with V_s with a coefficient of 0.4, quite independent of temperature and concentration.

This analysis quantifies wall slip in terms of b instead of V_s. Because the extrapolation length depends only on the viscosity and friction coefficient, it does not depend on kinematic variables and, therefore, can be considered a material property of the system. As the ratio b/D becomes larger, wall-slip corrections are necessary.

Comparing eqs 8 and 9, we find that the friction coefficient is related to the viscosity of the slip layer:

$$\beta = \frac{\eta_s}{\delta_s} \tag{12}$$

Therefore, the extrapolation length becomes

$$b = \frac{\eta}{\eta_s}\delta_s \tag{13}$$

According to eqs 9 and 10, the extrapolation length can be expressed in terms of the stress or shear rate. Because both V_s and the bulk shear rate vary as power laws with the stress, with a similar power-law index for high shear rates, eq 10 predicts a nearly constant b almost independent of the shear rate. The extrapolation length increases slowly with the stress, as shown in Figure 12, for several concentrations at 225 °C. Furthermore, because the extrapolation length depends very weakly on the shear rate, eq 10 states that the variation of the extrapolation length with V_s is almost linear (see Fig. 13). This regime was predicted by Brochard and de Gennes[15] and corresponds to the marginal regime, between the entangled and Rouse regimes, for a weakly grafted surface exposed to a polymer melt. In this case, as opposed to the one-component systems, because of the segregation observed in the micrographs between the core and the wall region, the grafted chains may be different from those in the core and represent those chains that are bound to the surface of the die.

The magnitudes of the extrapolation length are related to the magnitudes found in the microscopy studies for the slip-layer thickness through eq 13. The ratio of the viscosity in the bulk to that in the slip layer may be approximately 10–100. For $\delta_s \sim 1$ μm, the extrapolation length is 0.01–0.1 mm, which may not be negligibly small compared with the capillary diameter.

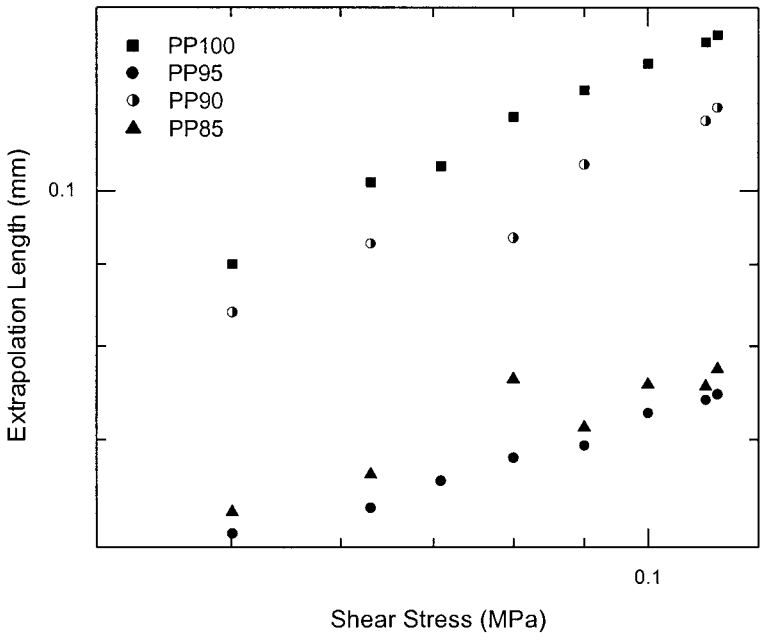

Figure 12. Extrapolation length as a function of the true shear stress for various blends at 225 °C.

DISCUSSION AND CONCLUDING REMARKS

In a study of the flow of PP and EVA in aluminum dies, Wang et al.[22] calculated extrapolation lengths from data taken in bare aluminum and coated dies. In the bare aluminum die, slip was not found in PP with the Mooney method. This is different from the results obtained in this work. The disagreement may be due to different molecular characteristics, such as tacticity (the sample used in this work was isotactic), molecular weight (228,000), and polydispersity (7.9 in this case). Also, the melt flow index may be different because

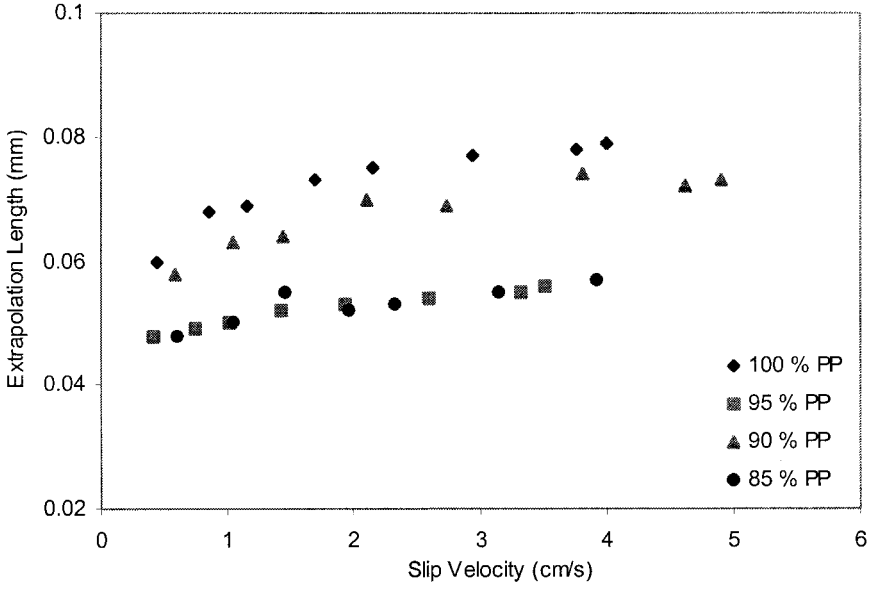

Figure 13. Extrapolation length versus the slip velocity for various blends at 225 °C.

the power-law coefficient of the flow curve in Wang et al.'s article is different from that of this work. Anyway, the slip we found in pure PP has a small magnitude and is smaller than that found in the blends with EVA throughout the composition range at 200 °C.

In Figure 11, the bulk data do not show any evidence of the slip–stick transition that is observed in polymer melts such as polyethylene. The highest stress attained according to Figure 11 is around 0.3 MPa, which is so low that no interfacial coil–stretch transition occurs. This is the reason why the rising branch of the flow curve at high shear rates observed in other works is absent. However, although the wall shear stresses are low, the dynamics of entanglement and disentanglement of chains at the wall differs from that of chains at the bulk, and this is enough to explain diameter-dependent flow curves, as the theoretical modeling of slip by Mashelkar et al.[2] has shown. Therefore, the observed development of the slip layer and the diameter-dependent flow curves in this polymer blend are due to the different dynamics of the bulk polymer and that of the polymer next to the wall.

Throughout the analysis presented here for the slip of a polymer blend in the melt state, we have emphasized the different dynamics occurring in the bulk and close to the wall. In fact, these dynamics reflect different rates of entanglement and disentanglement of chains. The consideration of this difference leads us to conclude that the nonmonotonic nature of the shear-stress/shear-rate curve arises from different rates of entanglement and disentanglement at the wall compared with that in the bulk.

Finally, the analysis of interfacial properties of the polymer was performed with two methods, and special care was taken to account for end effects (entrance effects) in the flow curves. V_s obtained by the Mooney method and the calculated extrapolation length led to same interpretations.

The authors acknowledge a grant from Consejo Nacional de Ciencia y Tecnología (CONACYT) through project G-27837U. The technical assistance of E. Sanchez, A. Caballero, S. Jimenez, M. T. Vázquez, and A. Luis is also acknowledged. The authors thank Dr. J. Pérez-González for stimulating discussions. A. Maciel thanks CONACYT (Reg. 114268) for its support.

REFERENCES AND NOTES

1. Wang, S. Q. Adv Polym Sci 1999, 138, 227–275.
2. Joshi, Y. M.; Lele, A. K.; Mashelkar, R. A. J Non-Newtonian Fluid Mech 2000, 89, 303–335.
3. Mooney, M. J Rheol 1931, 2, 210–222.
4. Whitlock, R. L.; Porter, R. S. J Polym Sci: Part A-2 1972, 10, 877–886.
5. Funatsu, K.; Sato, M. In Proceedings of the 9th International Congress on Rheology, Acapulco, Mexico, Mena, B.; García Rejón, A.; Rangel, C., Eds.; Universidad Nacional Autónoma de Mexico: México, 1984. Vol. 3, pp 539–541.
6. Knappe, W.; Krumböck, E. In Proceedings of the 9th International Congress on Rheology, Acapulco, Mexico, Mena, B.; García Rejón, A.; Rangel, C., Eds.; Universidad Nacional Autónoma de México: México, 1984. Vol. 3, pp 417–424.
7. Knappe, W.; Krumböck, E. Rheol Acta 1986, 25, 296–307.
8. Jiang, T. Q.; Young, A. C.; Metzner, A. B. Rheol Acta 1986, 25, 397–404.
9. Piau, J. M.; El Kissi, N.; Toussaint, F.; Mezghani, A. Rheol Acta 1995, 34, 40–57.
10. Wang, S. Q.; Drda, P. A. Macromolecules 1996, 29, 2627–2632.
11. Wang, S. Q.; Drda, P. A. Rheol Acta 1997, 36, 128–134.
12. De Vargas, L.; Manero, O. Polym Eng Sci 1989, 29, 1232–1237.
13. Pearson, J. R. A. J Rheol 1994, 38, 309–331.
14. Petri, C. S. J.; Denn, M. M. AIChE J 1976, 22, 209–236.
15. Brochard, F.; de Gennes, P. G. Langmuir 1992, 8, 3033–3037.
16. Valdez, M. A.; Yeomans, L.; Montes, F.; Acuña, H.; Ayala, A. Rheol Acta 1995, 34, 474–482.
17. Jiang, T. Q.; Young, A. C.; Metzner, A. B. Rheol Acta 1986, 25, 397–404.
18. Gupta, A. K.; Ratnam, B. K.; Srinivasan, R. J Appl Polym Sci 1992, 46, 281–293.
19. Joshi, M.; Misra, A.; Maiti, S. N. J Appl Polym Sci 1991, 43, 311–328.
20. Petrovic, Z. S.; Budinski-Simendic, J.; Divjakovic, V. J Appl Polym Sci 1991, 42, 779–790.
21. Chen, H. L.; Porter, R. S. Polym Eng Sci 1992, 32, 1870–1875.
22. Yang, X.; Ishida, H.; Wang, S. J Rheol 1998, 42, 63–80.